Design and synthesis of metal-based chemotherapeutic agents for targeted DNA interactions or DNA repair pathway modulation

Griend, C.J. van de

Appendix I: supporting information for chapter 2

pK_a determination

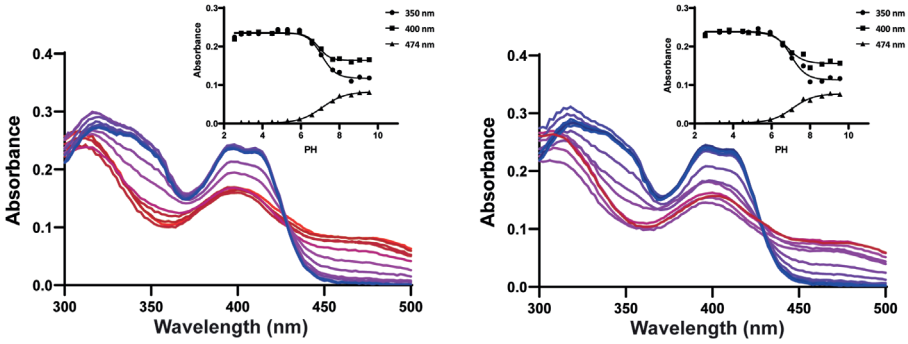

Figure SI.1. Absorption spectra at variable pH for $[Pt(H_2\mathbf{L1})](Cl)_2$. The blue/red gradient represents the range from acidic to basic conditions, respectively.

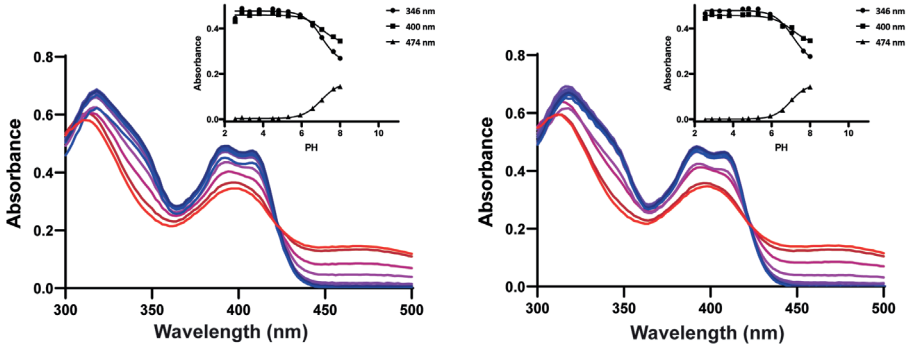

Figure SI.2. Absorption spectra at variable pH for $[Pt(H_2\mathbf{L2})](Cl)_2$. The blue/red gradient represents the range from acidic to basic conditions, respectively.

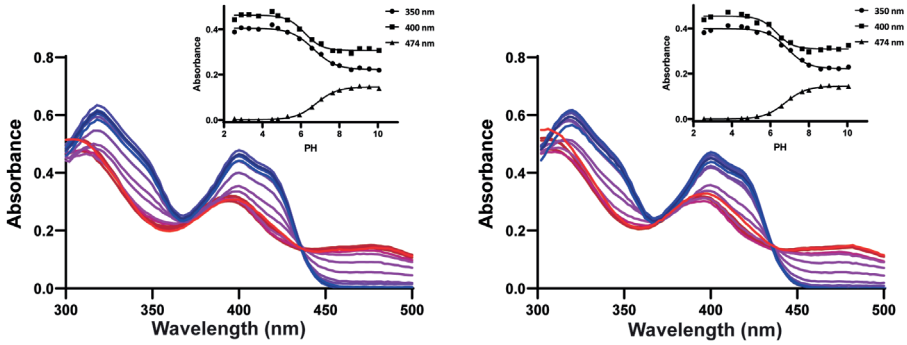

Figure SI.3. Absorption spectra at variable pH for $[Pt(H_2\mathbf{L3})](Cl)_2$. The blue/red gradient represents the range from acidic to basic conditions, respectively.

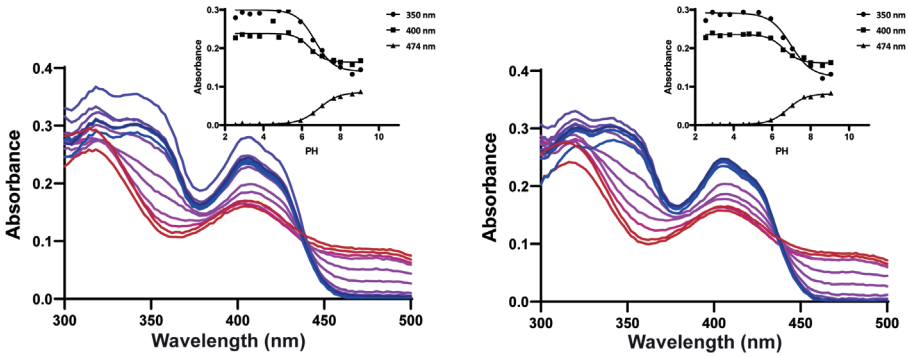

Figure SI.4. Absorption spectra at variable pH for [Pt(H_2**L4**)]$(Cl)_2$. The blue/red gradient represents the range from acidic to basic conditions, respectively.

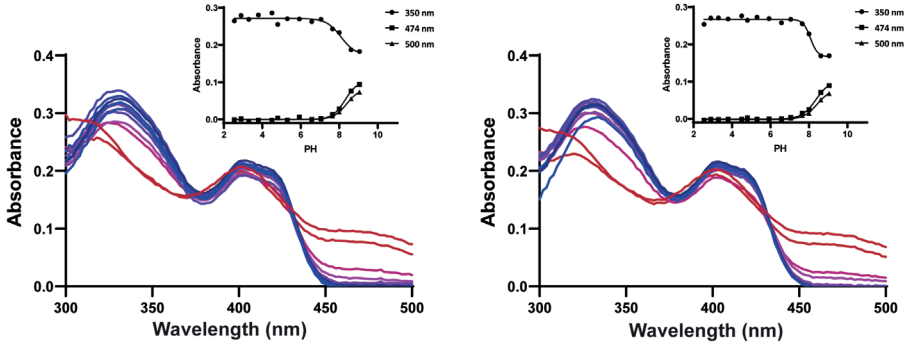

Figure SI.5. Absorption spectra at variable pH for [Pt(H_2**L5**)]$(Cl)_2$. The blue/red gradient represents the range from acidic to basic conditions, respectively.

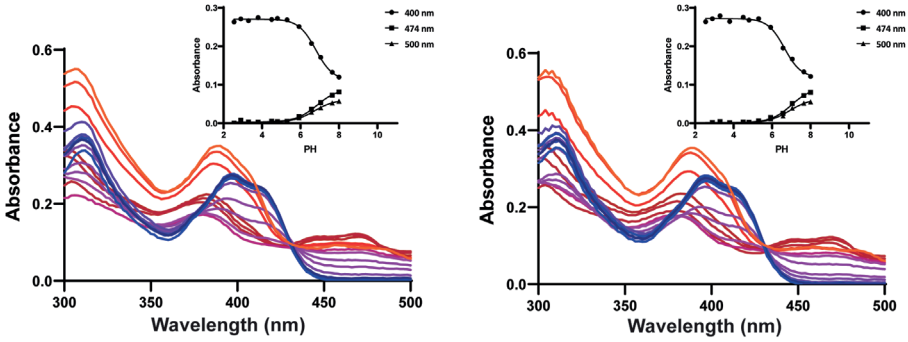

Figure SI.6. Absorption spectra at variable pH for [Pt(H_2**L6**)]$(Cl)_2$. The blue/red gradient represents the range from acidic to basic conditions, respectively.

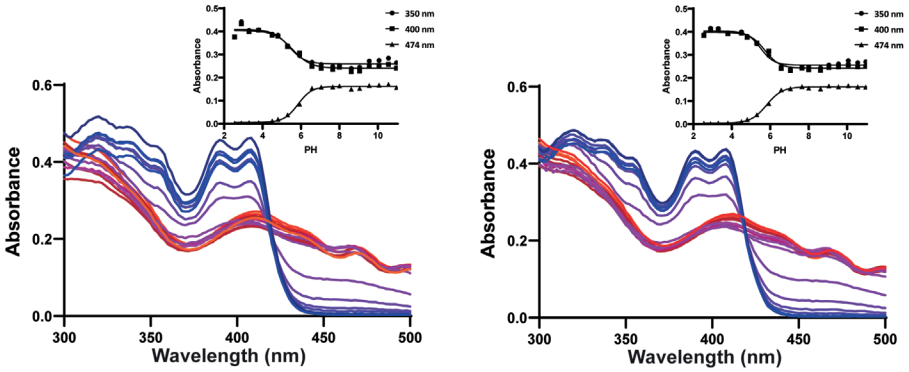

Figure SI.7. Absorption spectra at variable pH for [Pt(H_2**L7**)]$(Cl)_2$. The blue/red gradient represents the range from acidic to basic conditions, respectively.

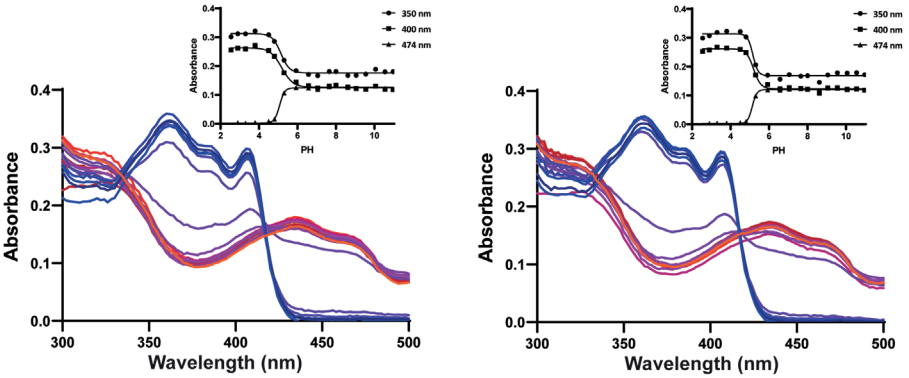

Figure SI.8. Absorption spectra at variable pH for [Pt(H_2**L8**)]$(Cl)_2$. The blue/red gradient represents the range from acidic to basic conditions, respectively.

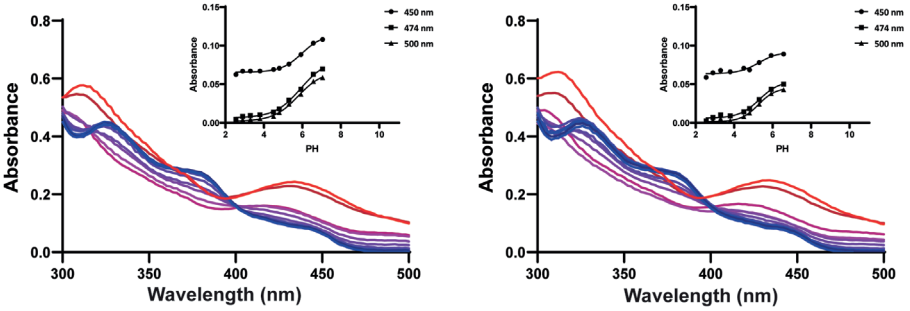

Figure SI.9. Absorption spectra at variable pH for [Pt(H_2**L9**)]$(Cl)_2$. The blue/red gradient represents the range from acidic to basic conditions, respectively.

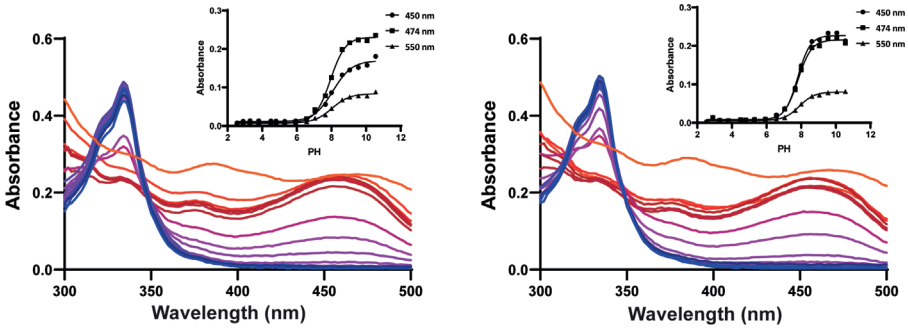

Figure SI.10. Absorption spectra at variable pH for [Pt(H_2**L13**)](PF_6)$_2$. The blue/red gradient represents the range from acidic to basic conditions, respectively.

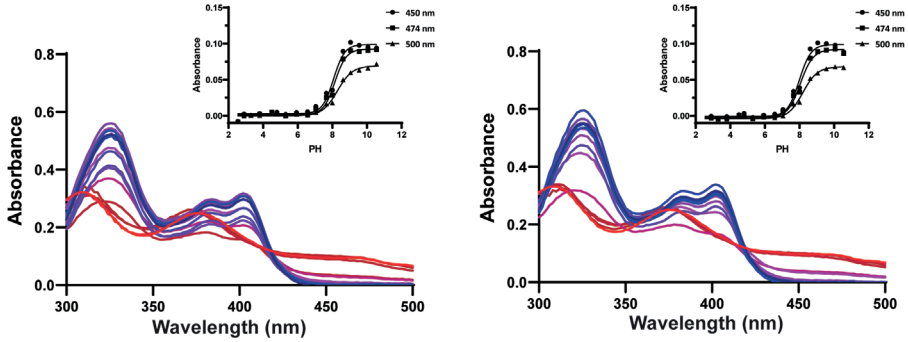

Figure SI.11. Absorption spectra at variable pH for [Pd(H_2**L1**)](Cl)$_2$. The blue/red gradient represents the range from acidic to basic conditions, respectively.

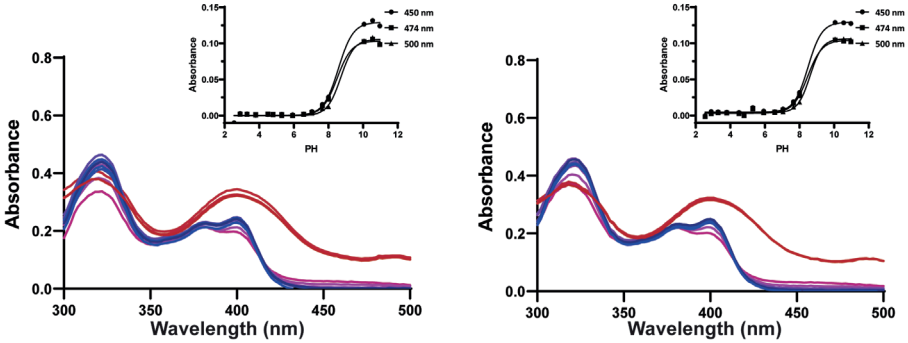

Figure SI.12. Absorption spectra at variable pH for [Pd(H2L2)](Cl)2. The blue/red gradient represents the range from acidic to basic conditions, respectively.

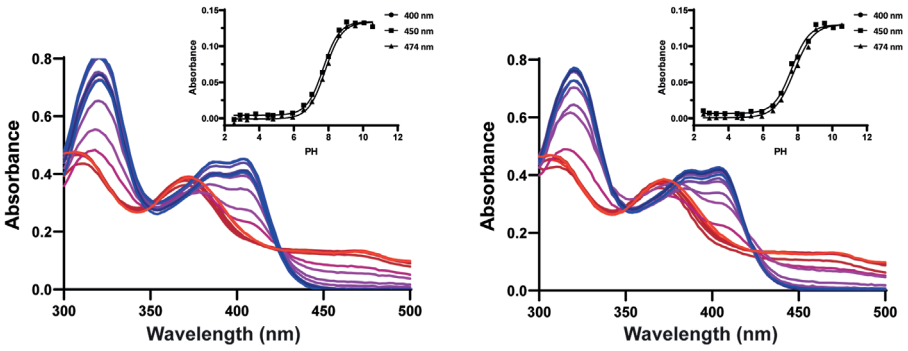

Figure SI.13. Absorption spectra at variable pH for [Pd(H_2**L3**)]$(Cl)_2$. The blue/red gradient represents the range from acidic to basic conditions, respectively.

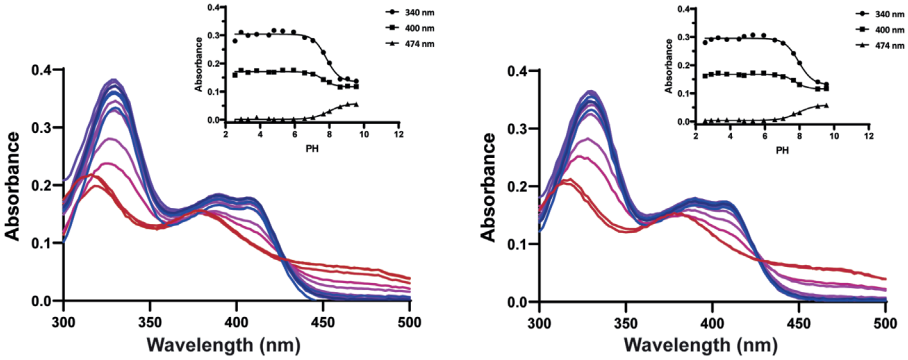

Figure SI.14. Absorption spectra at variable pH for [Pd(H_2**L4**)]$(Cl)_2$. The blue/red gradient represents the range from acidic to basic conditions, respectively.

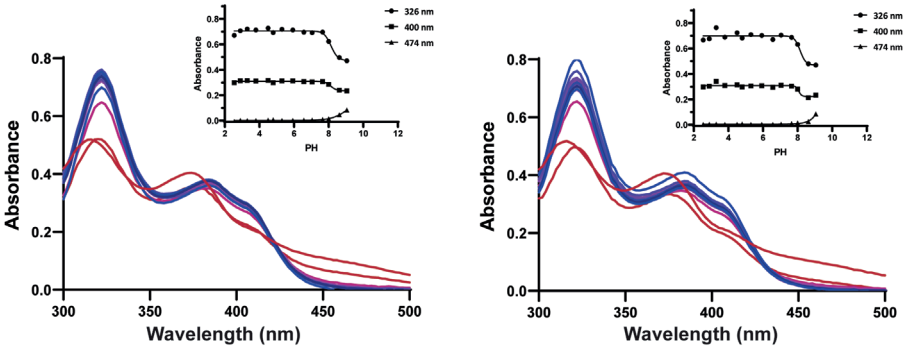

Figure SI.15. Absorption spectra at variable pH for [Pd(H_2**L5**)]$(Cl)_2$. The blue/red gradient represents the range from acidic to basic conditions, respectively.

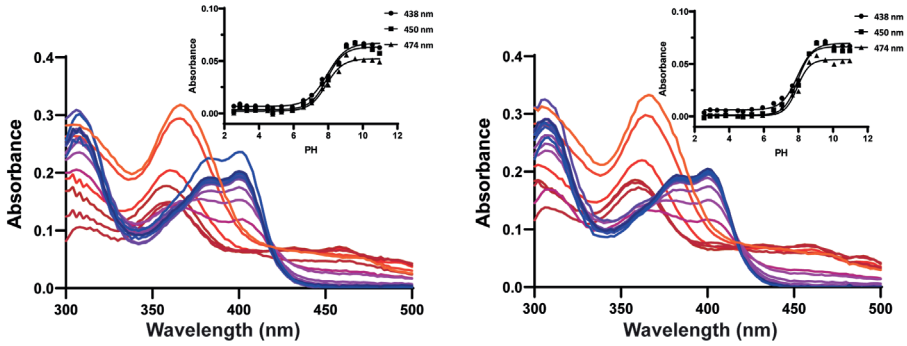

Figure SI.16. Absorption spectra at variable pH for [Pd(H_2**L6**)]$(Cl)_2$. The blue/red gradient represents the range from acidic to basic conditions, respectively.

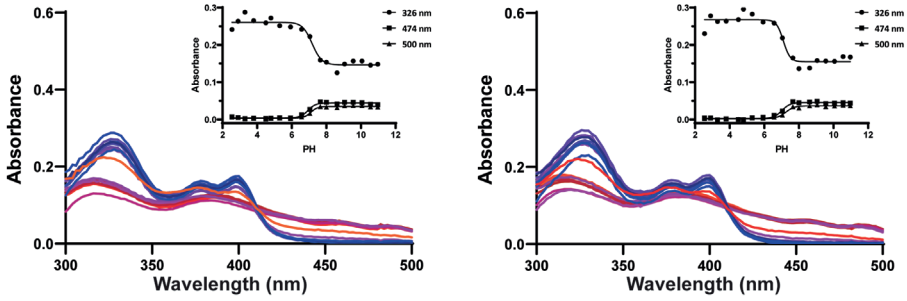

Figure SI.17. Absorption spectra at variable pH for [Pd(H_2**L7**)]$(Cl)_2$. The blue/red gradient represents the range from acidic to basic conditions, respectively.

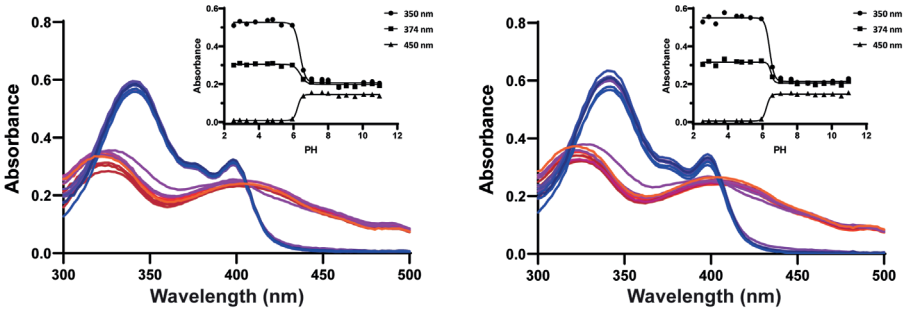

Figure SI.18. Absorption spectra at variable pH for [Pd(H_2**L8**)]$(Cl)_2$. The blue/red gradient represents the range from acidic to basic conditions, respectively.

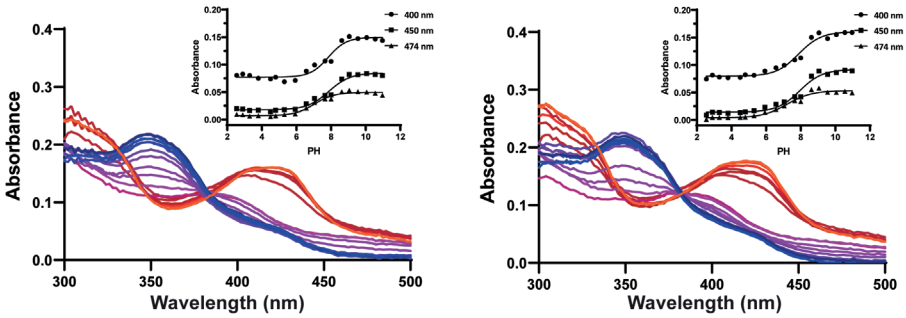

Figure SI.19. Absorption spectra at variable pH for [Pd(H_2**L9**)]$(Cl)_2$. The blue/red gradient represents the range from acidic to basic conditions, respectively.

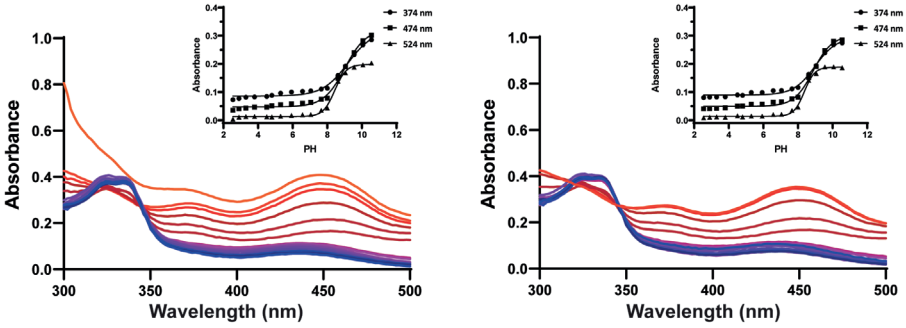

Figure SI.20. Absorption spectra at variable pH for [Pd(H_2**L13**)]$(Cl)_2$. The blue/red gradient represents the range from acidic to basic conditions, respectively.

pUC19 Agarose gel electrophoresis

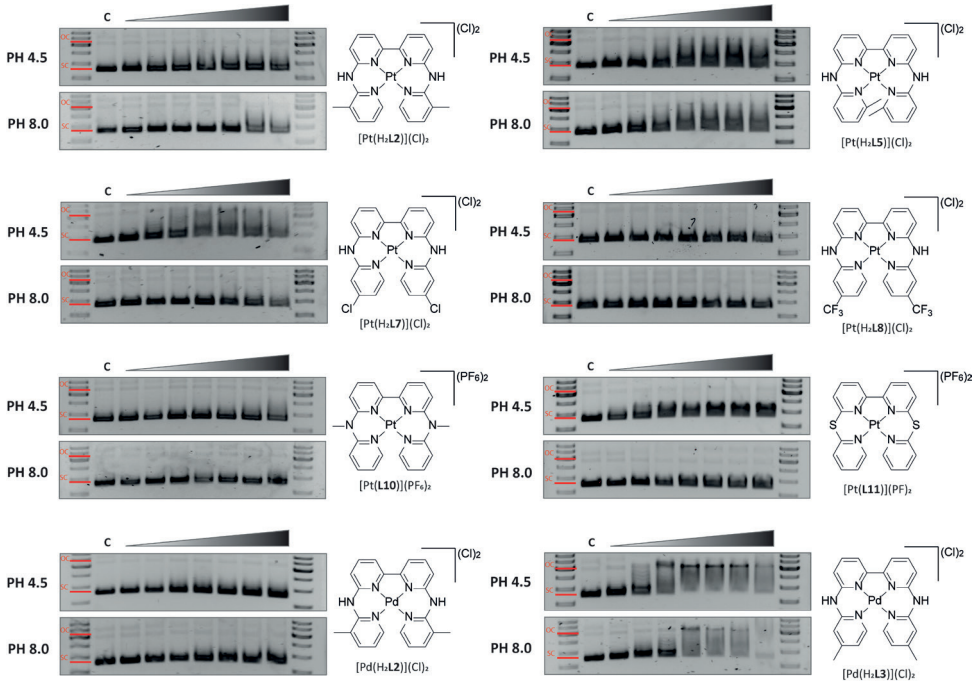

Figure SI.21. Agarose gel electrophoresis analysis of the interactions of pUC19 plasmid DNA and metal complexes at pH 4.5 and 8. Lane 1 and 10 contain the molecular ladders, lane 2 is the pUC19 DNA plasmid only control and lane 3-9 contained increasing metal complex (MC) to base pair (BP) concentration ratios (0.05, 0.1, 0.2, 0.5, 1, 2, 5).

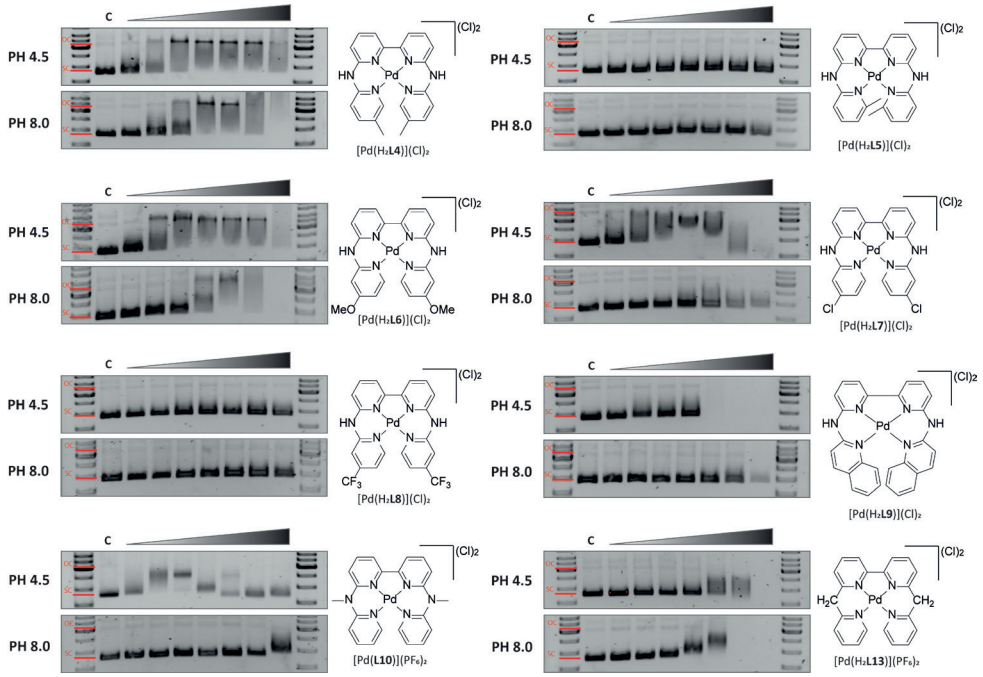

Figure SI.22. Agarose gel electrophoresis analysis of the interactions of pUC19 plasmid DNA and metal complexes at pH 4.5 and 8. Lane 1 and 10 contain the molecular ladders, lane 2 is the pUC19 DNA plasmid only control and lane 3-9 contained increasing metal complex (MC) to base pair (BP) concentration ratios (0.05, 0.1, 0.2, 0.5, 1, 2, 5).

I

Titration of $[M(H_2LX)]^{2+}$ complexes with calf thymus DNA analyzed by plate reader.

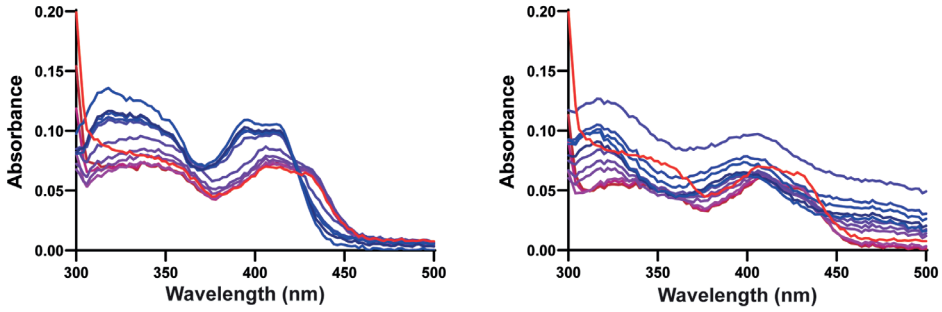

Figure SI.23. Calf thymus titration absorbance spectra of $[Pt(H_2\mathbf{L1})](Cl)_2$ (33 µm) at pH 5 (left) and pH 8 (right). The blue to red gradient represents increasing DNA concentration range from 0 to 666 µm basepairs, respectively.

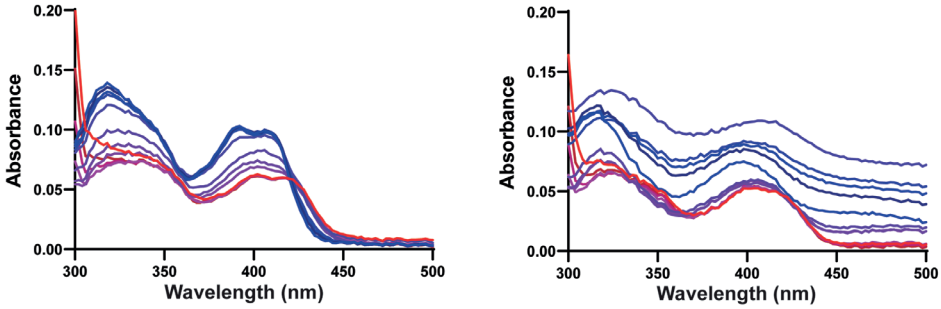

Figure SI.24. Calf thymus titration absorbance spectra of [Pt(H_2**L2**)]$(Cl)_2$ (33 µm) at pH 5 (left) and pH 8 (right). The blue to red gradient represents increasing DNA concentration range from 0 to 666 µm basepairs, respectively.

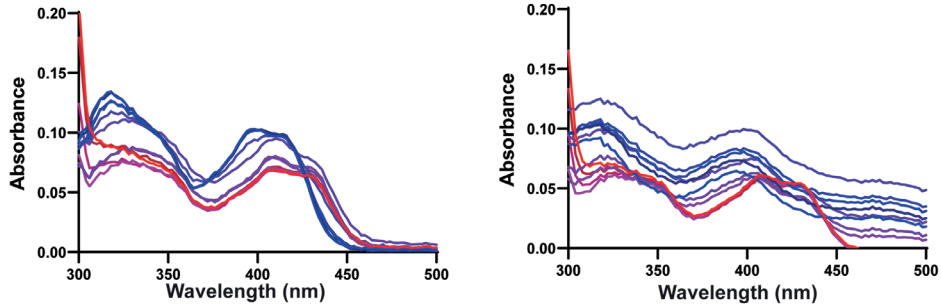

Figure SI.25. Calf thymus titration absorbance spectra of [Pt(H_2**L3**)]$(Cl)_2$ (33 µm) at pH 5 (left) and pH 8 (right). The blue to red gradient represents increasing DNA concentration range from 0 to 666 µm basepairs, respectively.

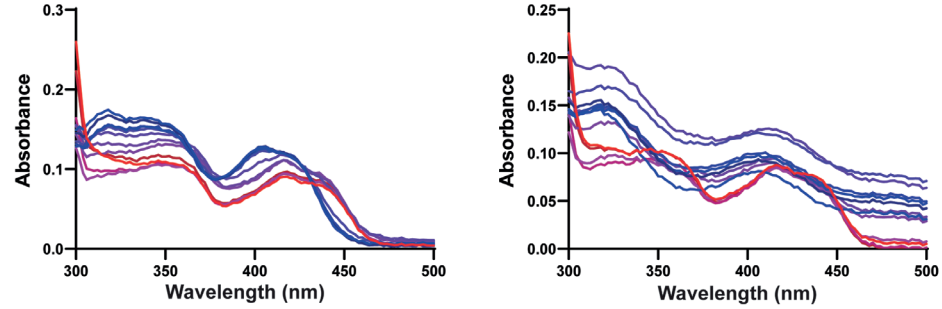

Figure SI.26. Calf thymus titration absorbance spectra of [Pt(H_2**L4**)]$(Cl)_2$ (33 µm) at pH 5 (left) and pH 8 (right). The blue to red gradient represents increasing DNA concentration range from 0 to 666 µm basepairs, respectively.

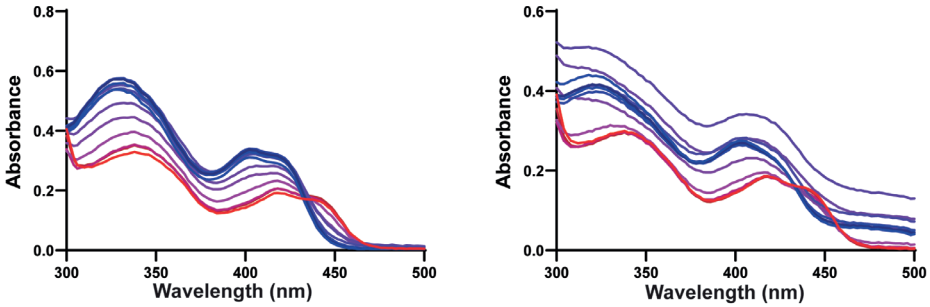

Figure SI.27. Calf thymus titration absorbance spectra of [Pt(H_2**L5**)]($Cl)_2$ (33 µm) at pH 5 (left) and pH 8 (right). The blue to red gradient represents increasing DNA concentration range from 0 to 666 µm basepairs, respectively.

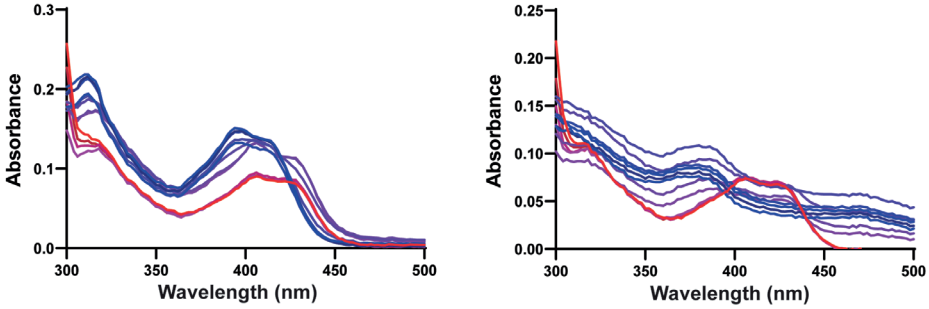

Figure SI.28. Calf thymus titration absorbance spectra of [Pt(H_2**L6**)]($Cl)_2$ (33 µm) at pH 5 (left) and pH 8 (right). The blue to red gradient represents increasing DNA concentration range from 0 to 666 µm basepairs, respectively.

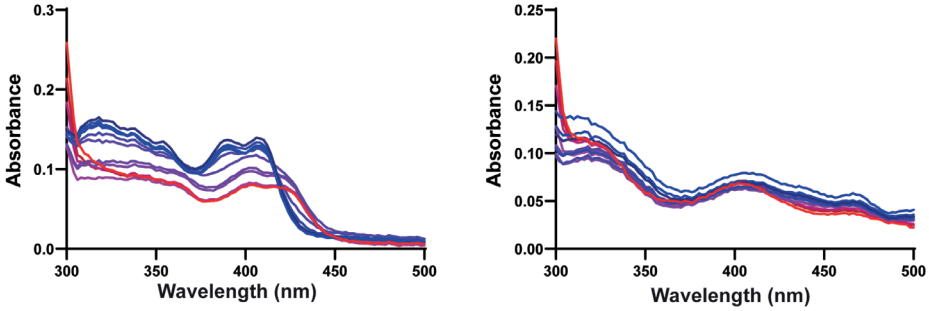

Figure SI.29. Calf thymus titration absorbance spectra of [Pt(H_2**L7**)]($Cl)_2$ (33 µm) at pH 5 (left) and pH 8 (right). The blue to red gradient represents increasing DNA concentration range from 0 to 666 µm basepairs, respectively.

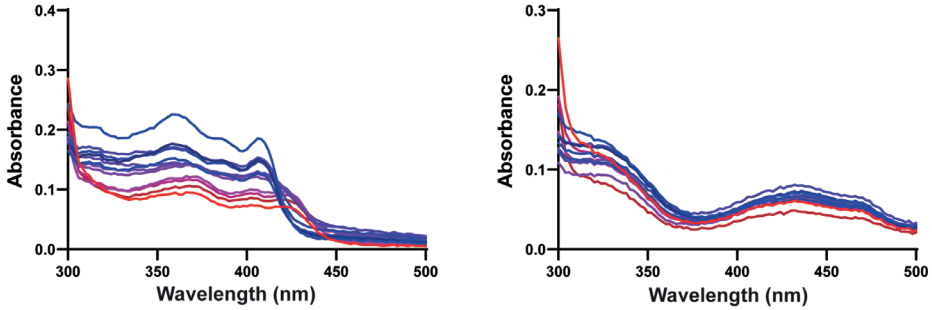

Figure SI.30. Calf thymus titration absorbance spectra of [Pt(H_2**L8**)]($Cl)_2$ (33 µm) at pH 5 (left) and pH 8 (right). The blue to red gradient represents increasing DNA concentration range from 0 to 666 µm basepairs, respectively.

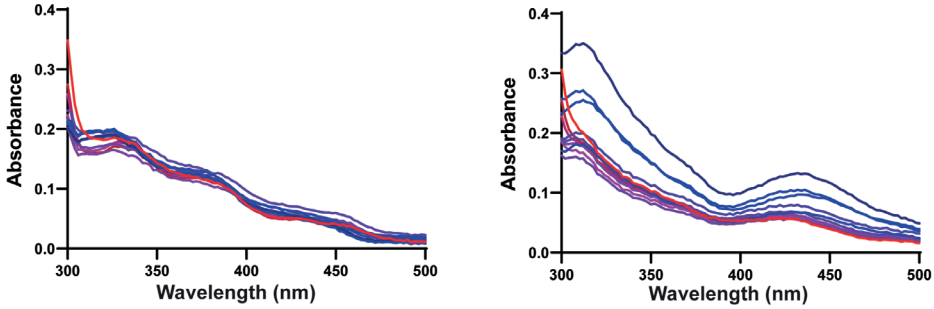

Figure SI.31. Calf thymus titration absorbance spectra of [Pt(H_2**L9**)]($Cl)_2$ (33 µm) at pH 5 (left) and pH 8 (right). The blue to red gradient represents increasing DNA concentration range from 0 to 666 µm basepairs, respectively.

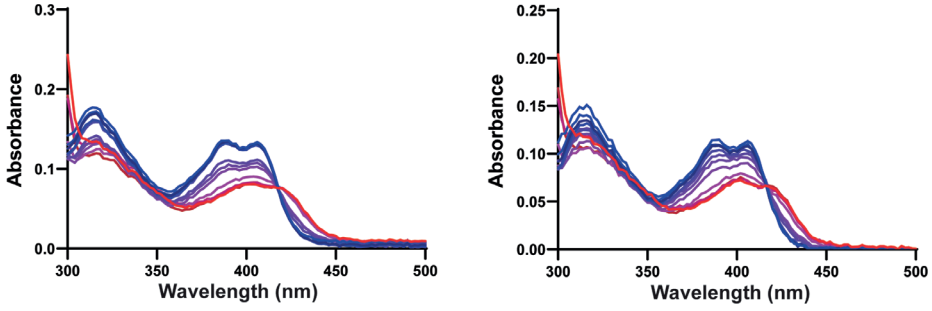

Figure SI.32. Calf thymus titration absorbance spectra of [Pt(**L10**)]($PF_6)_2$ (33 µm) at pH 5 (left) and pH 8 (right). The blue to red gradient represents increasing DNA concentration range from 0 to 666 µm basepairs, respectively.

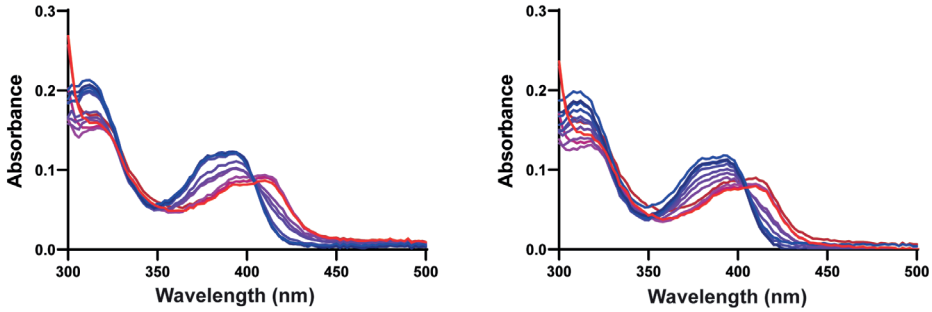

Figure SI.33. Calf thymus titration absorbance spectra of [Pt(**L11**)]$(PF_6)_2$ (33 µm) at pH 5 (left) and pH 8 (right). The blue to red gradient represents increasing DNA concentration range from 0 to 666 µm basepairs, respectively.

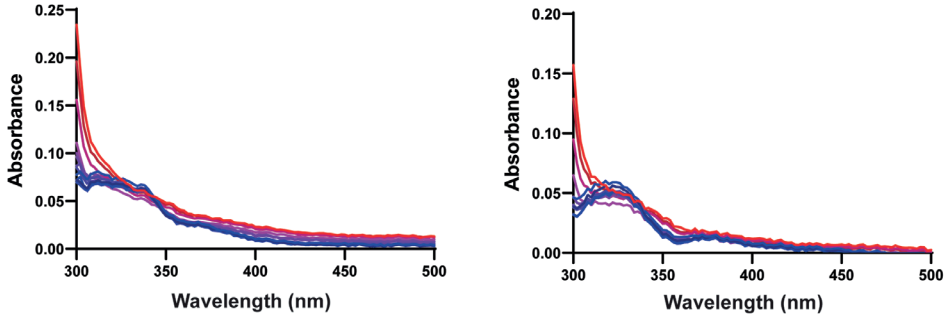

Figure SI.34. Calf thymus titration absorbance spectra of [Pt(**L12**)]$(Cl)_2$ (33 µm) at pH 5 (left) and pH 8 (right). The blue to red gradient represents increasing DNA concentration range from 0 to 666 µm basepairs, respectively.

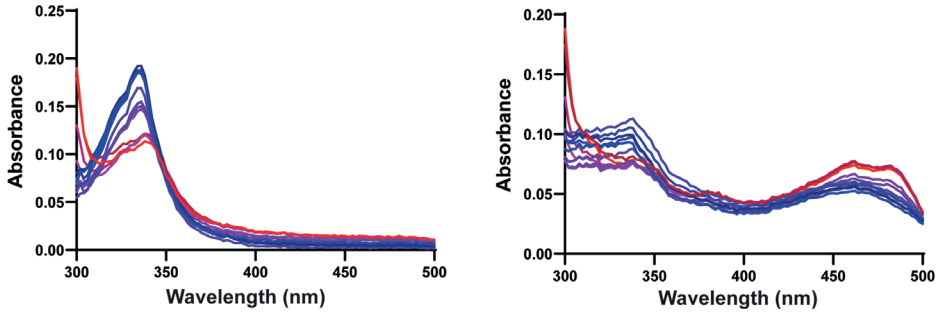

Figure SI.35. Calf thymus titration absorbance spectra of [Pt(H_2**L13**)]$(PF_6)_2$ (33 µm) at pH 5 (left) and pH 8 (right). The blue to red gradient represents increasing DNA concentration range from 0 to 666 µm basepairs, respectively.

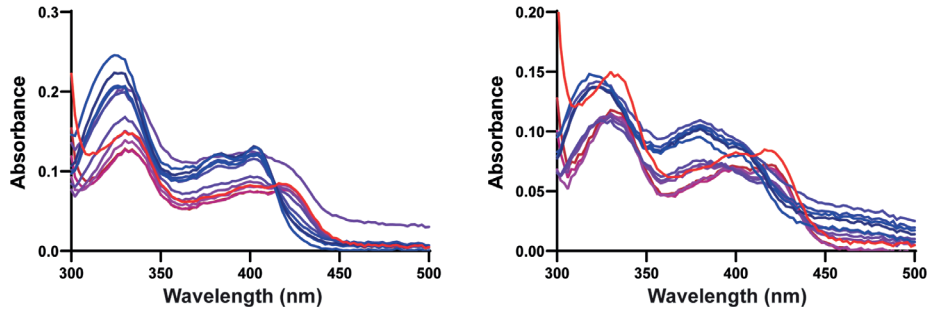

Figure SI.36. Calf thymus titration absorbance spectra of [Pd(H_2**L1**)]$(Cl)_2$ (33 µm) at pH 5 (left) and pH 8 (right). The blue to red gradient represents increasing DNA concentration range from 0 to 666 µm basepairs, respectively.

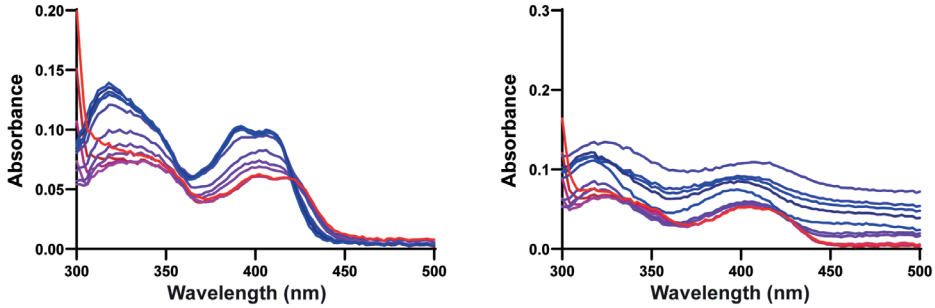

Figure SI.37. Calf thymus titration absorbance spectra of [Pd(H_2**L2**)]$(Cl)_2$ (33 µm) at pH 5 (left) and pH 8 (right). The blue to red gradient represents increasing DNA concentration range from 0 to 666 µm basepairs, respectively.

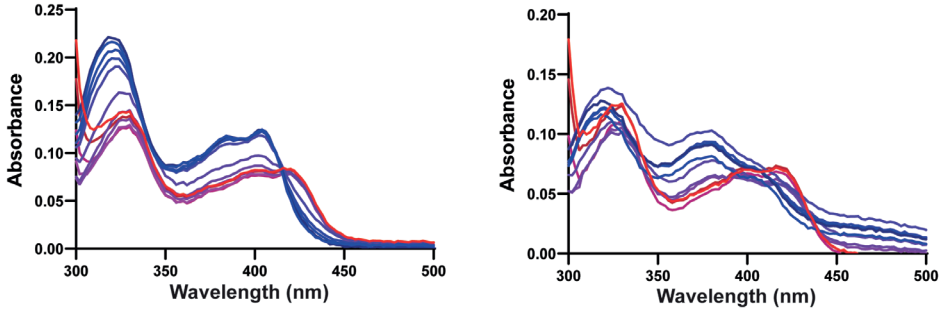

Figure SI.38. Calf thymus titration absorbance spectra of [Pd(H_2**L3**)]$(Cl)_2$ (33 µm) at pH 5 (left) and pH 8 (right). The blue to red gradient represents increasing DNA concentration range from 0 to 666 µm basepairs, respectively.

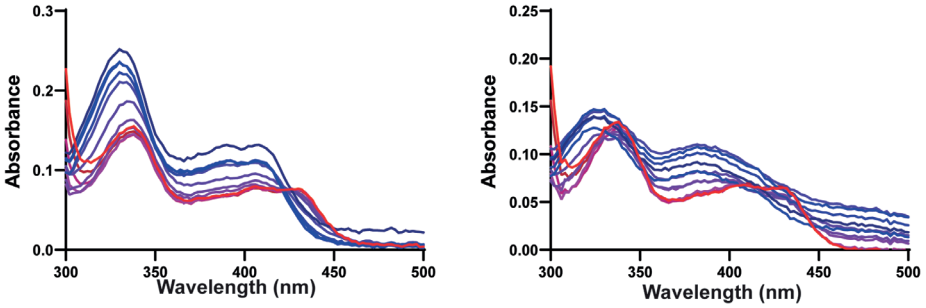

Figure SI.39. Calf thymus titration absorbance spectra of [Pd(H_2**L4**)]$(Cl)_2$ (33 µm) at pH 5 (left) and pH 8 (right). The blue to red gradient represents increasing DNA concentration range from 0 to 666 µm basepairs, respectively.

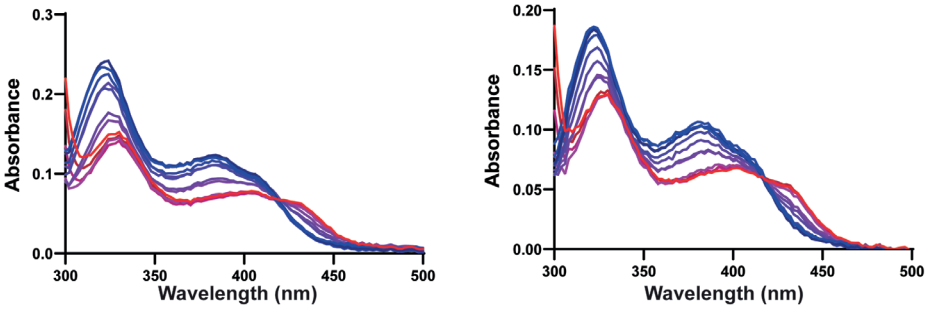

Figure SI.40. Calf thymus titration absorbance spectra of [Pd(H_2**L5**)]$(Cl)_2$ (33 µm) at pH 5 (left) and pH 8 (right). The blue to red gradient represents increasing DNA concentration range from 0 to 666 µm basepairs, respectively.

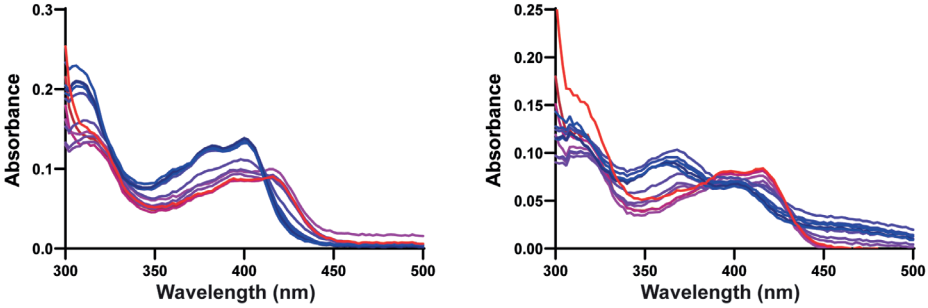

Figure SI.41. Calf thymus titration absorbance spectra of [Pd(H_2**L6**)]$(Cl)_2$ (33 µm) at pH 5 (left) and pH 8 (right). The blue to red gradient represents increasing DNA concentration range from 0 to 666 µm basepairs, respectively.

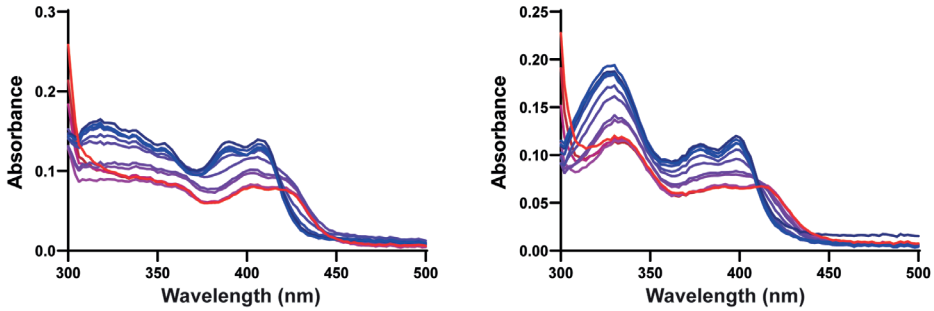

Figure SI.42. Calf thymus titration absorbance spectra of [Pd(H_2**L7**)]$(Cl)_2$ (33 µm) at pH 5 (left) and pH 8 (right). The blue to red gradient represents increasing DNA concentration range from 0 to 666 µm basepairs, respectively.

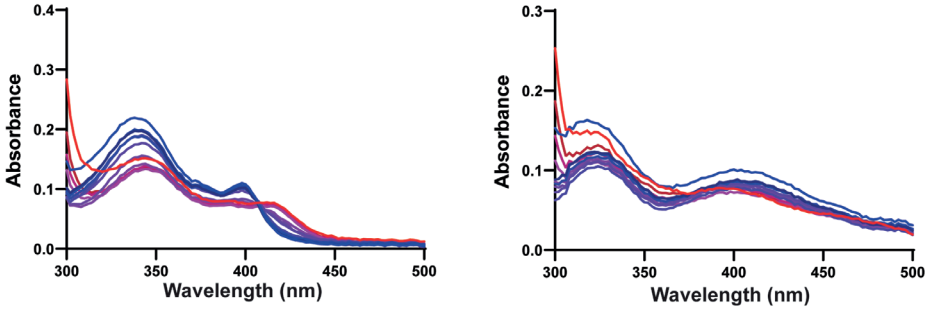

Figure SI.43. Calf thymus titration absorbance spectra of [Pd(H_2**L8**)]$(Cl)_2$ (33 µm) at pH 5 (left) and pH 8 (right). The blue to red gradient represents increasing DNA concentration range from 0 to 666 µm basepairs, respectively.

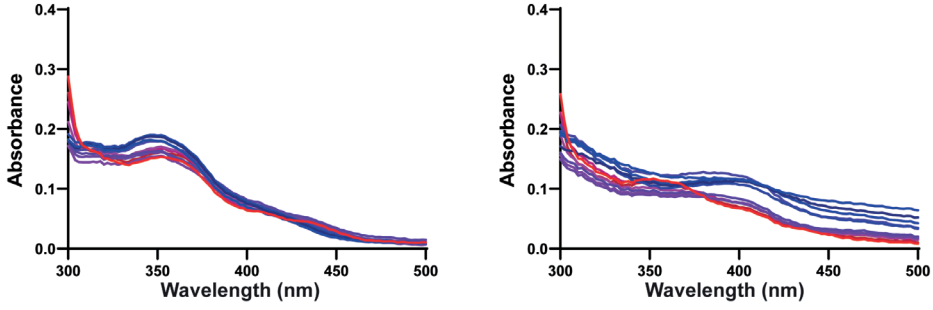

Figure SI.44. Calf thymus titration absorbance spectra of [Pd(H_2**L9**)]$(Cl)_2$ (33 µm) at pH 5 (left) and pH 8 (right). The blue to red gradient represents increasing DNA concentration range from 0 to 666 µm basepairs, respectively.

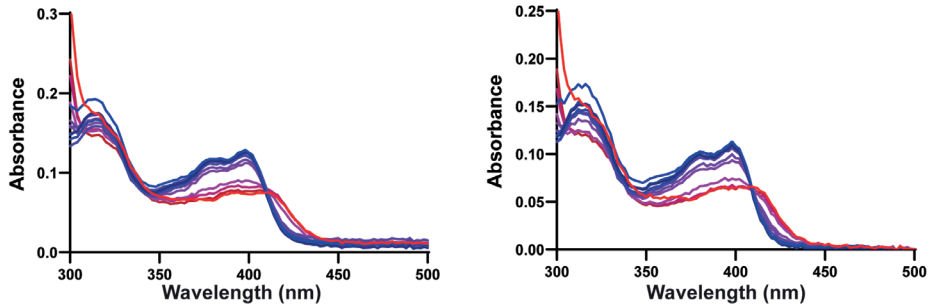

Figure SI.45. Calf thymus titration absorbance spectra of [Pd(**L10**)]$(Cl)_2$ (33 µm) at pH 5 (left) and pH 8 (right). The blue to red gradient represents increasing DNA concentration range from 0 to 666 µm basepairs, respectively.

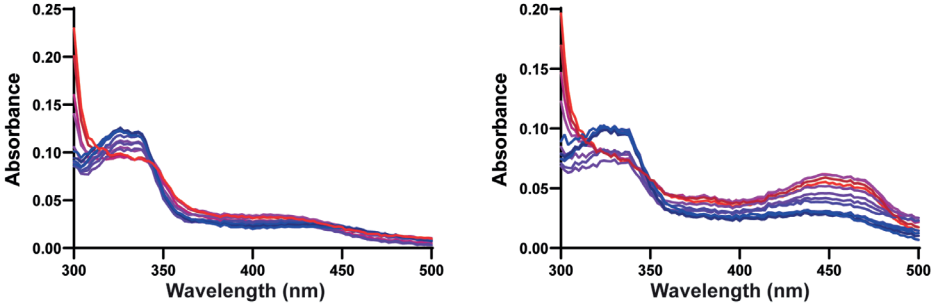

Figure SI.46. Calf thymus titration absorbance spectra of [Pd(H_2**L13**)]$(Cl)_2$ (33 µm) at pH 5 (left) and pH 8 (right). The blue to red gradient represents increasing DNA concentration range from 0 to 666 µm basepairs, respectively.

Binding constant determination of $[M(H_2LX)]^{2+}$ complexes to calf thymus DNA

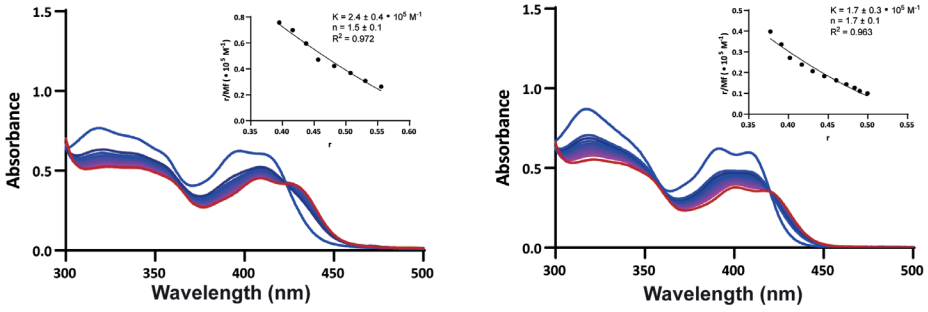

Figure SI.47. Calf thymus titration absorbance spectra of 100 µm [Pt(H_2**L1**)]$(Cl)_2$ (left) and [Pt(H_2**L2**)]$(Cl)_2$ (right) at pH 4.5. The blue to red gradient represents increasing DNA concentration from 0 to 360 µm basepairs, respectively. The inlays are Scatchard plots fitted to the McGhee–von Hippel model.

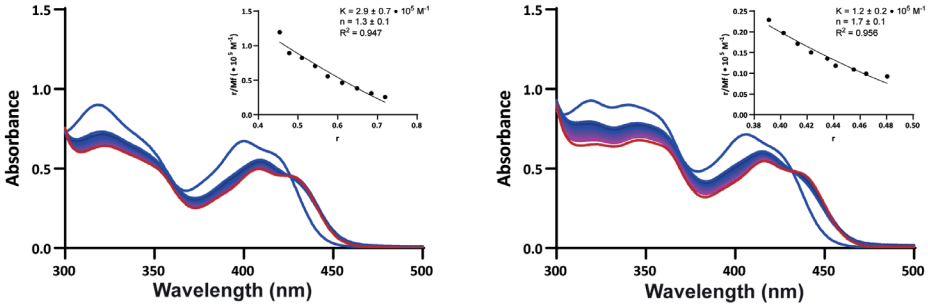

Figure SI.48. Calf thymus titration absorbance spectra of 100 µm $[Pt(H_2\mathbf{L3})](Cl)_2$ (left) and $[Pt(H_2\mathbf{L4})](Cl)_2$ (right) at pH 4.5. The blue to red gradient represents increasing DNA concentration from 0 to 360 µm base-pairs, respectively. The inlays are Scatchard plots fitted to the McGhee–von Hippel model.

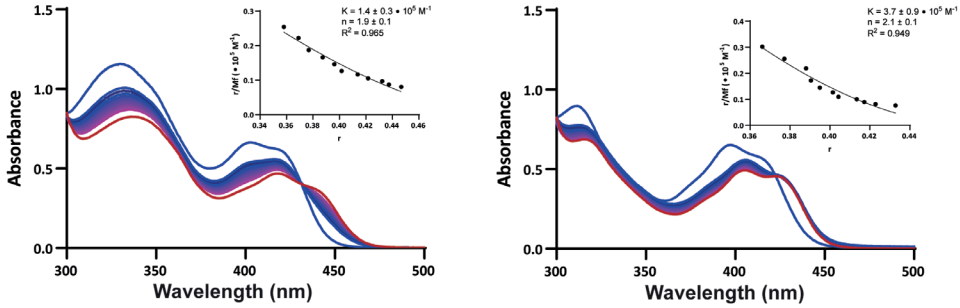

Figure SI.49. Calf thymus titration absorbance spectra of 100 µm $[Pt(H_2\mathbf{L5})](Cl)_2$ (left) and $[Pt(H_2\mathbf{L6})](Cl)_2$ (right) at pH 4.5. The blue to red gradient represents increasing DNA concentration from 0 to 360 µm base-pairs, respectively. The inlays are Scatchard plots fitted to the McGhee–von Hippel model.

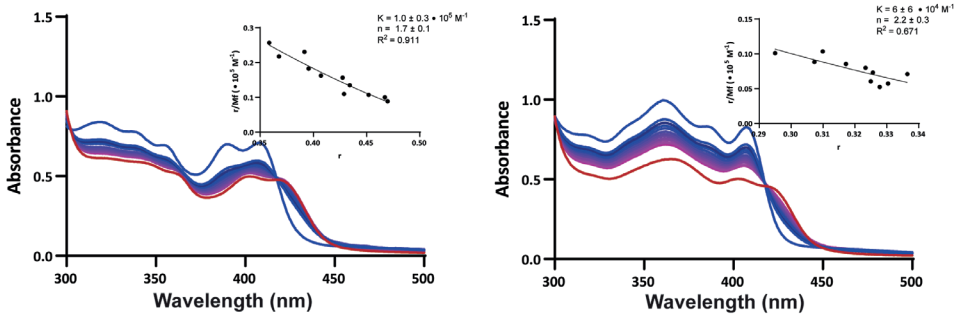

Figure SI.50. Calf thymus titration absorbance spectra of 100 µm $[Pt(H_2\mathbf{L7})](Cl)_2$ (left) and $[Pt(H_2\mathbf{L8})](Cl)_2$ (right) at pH 4.5. The blue to red gradient represents increasing DNA concentration from 0 to 360 µm base-pairs, respectively. The inlays are Scatchard plots fitted to the McGhee–von Hippel model.

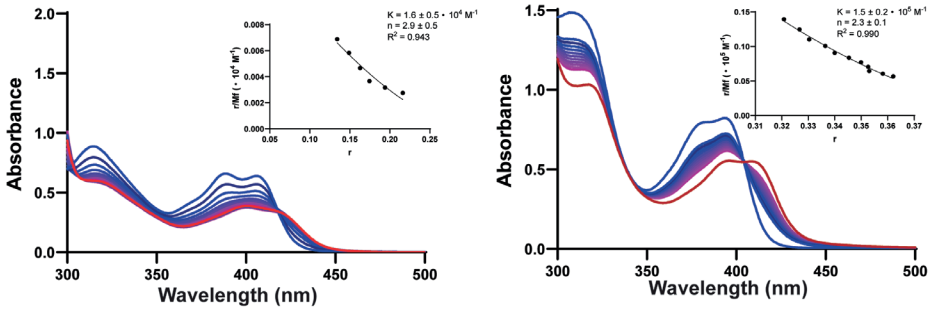

Figure SI.51. Calf thymus titration absorbance spectra of 100 µm [Pt(**L10**)]$(PF_6)_2$ (left) and [Pt(**L11**)]$(PF_6)_2$ (right) at pH 4.5. The blue to red gradient represents increasing DNA concentration from 0 to 1000 µm base-pairs for [Pt(**L10**)]$(PF_6)_2$ and 0 to 360 µm basepairs for [Pt(**L11**)]$(PF_6)_2$, respectively. The inlays are Scatchard plots fitted to the McGhee–von Hippel model.

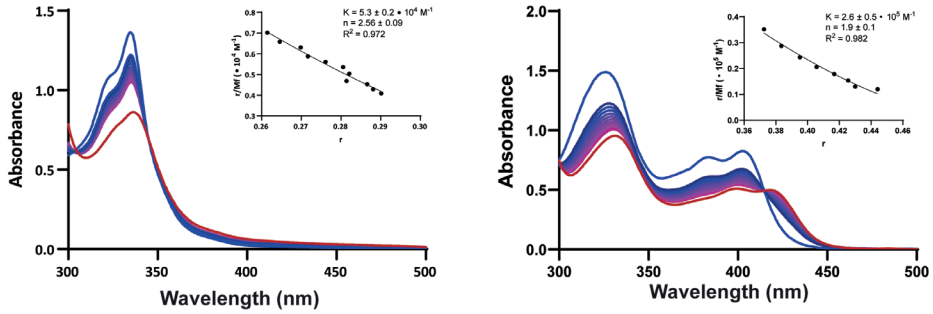

Figure SI.52. Calf thymus titration absorbance spectra of 100 µm [Pt(H_2**L13**)]$(PF_6)_2$ (left) and [Pd(H_2**L1**)]$(Cl)_2$ (right) at pH 4.5. The blue to red gradient represents increasing DNA concentration from 0 to 360 µm base-pairs, respectively. The inlays are Scatchard plots fitted to the McGhee–von Hippel model.

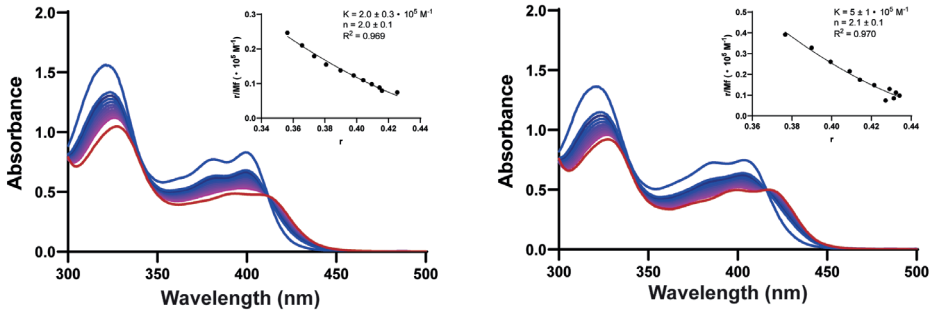

Figure SI.53. Calf thymus titration absorbance spectra of 100 µm [Pd(H_2**L2**)]$(PF_6)_2$ (left) and [Pd(H_2**L3**)]$(Cl)_2$ (right) at pH 4.5. The blue to red gradient represents increasing DNA concentration from 0 to 360 µm base-pairs, respectively. The inlays are Scatchard plots fitted to the McGhee–von Hippel model.

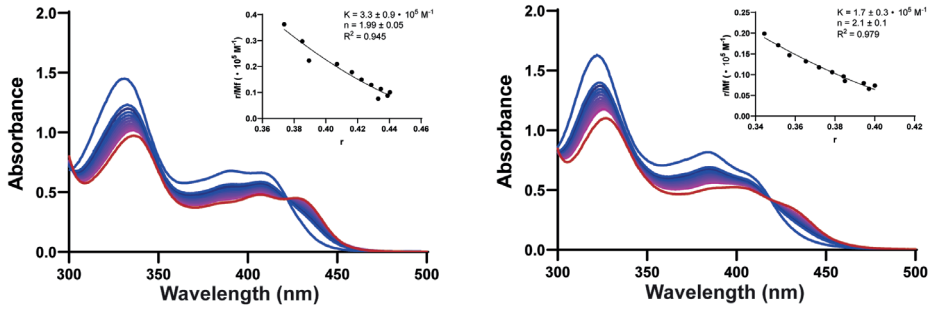

Figure SI.54. Calf thymus titration absorbance spectra of 100 µm [Pd(H_2**L4**)](PF_6)$_2$ (left) and [Pd(H_2**L5**)](Cl)$_2$ (right) at pH 4.5. The blue to red gradient represents increasing DNA concentration from 0 to 360 µm basepairs, respectively. The inlays are Scatchard plots fitted to the McGhee–von Hippel model.

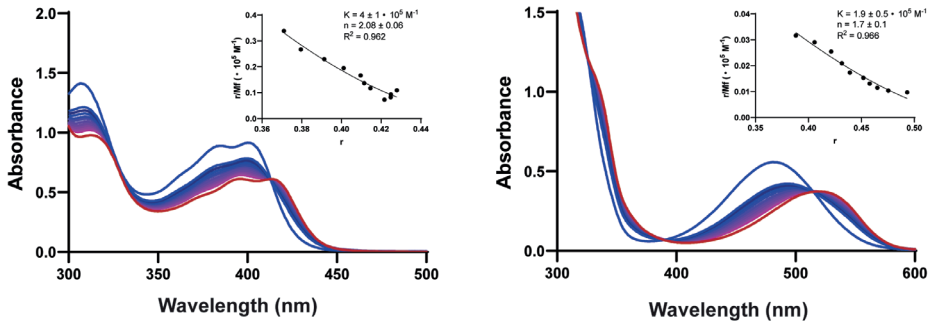

Figure SI.55. Calf thymus titration absorbance spectra of 100 µm [Pd(H_2**L6**)](PF_6)$_2$ (left) and ethidium bromide (right) at pH 4.5. The blue to red gradient represents increasing DNA concentration from 0 to 360 µm basepairs, respectively. The inlay is a Scatchard plots fitted to the McGhee–von Hippel model.

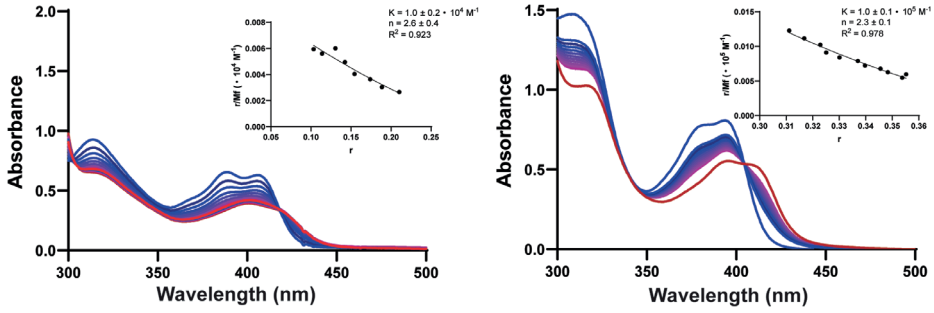

Figure SI.56. Calf thymus titration absorbance spectra of 100 µm [Pt(**L10**)](PF_6)$_2$ (left) and [Pt(**L11**)](PF_6)$_2$ (right) at pH 8. The blue to red gradient represents increasing DNA concentration from 0 to 360 µm basepairs, respectively. The inlay is a Scatchard plots fitted to the McGhee–von Hippel model.

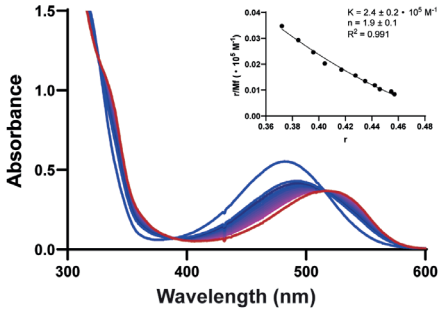

Figure SI.57. Calf thymus titration absorbance spectra of 100 µm ethidium bromide at pH 8. The blue to red gradient represents increasing DNA concentration from 0 to 360 µm basepairs, respectively. The inlay is a Scatchard plots fitted to the McGhee–von Hippel model.

Appendix II: supporting information for chapter 3

Crystal structures of diastereomers and epimers

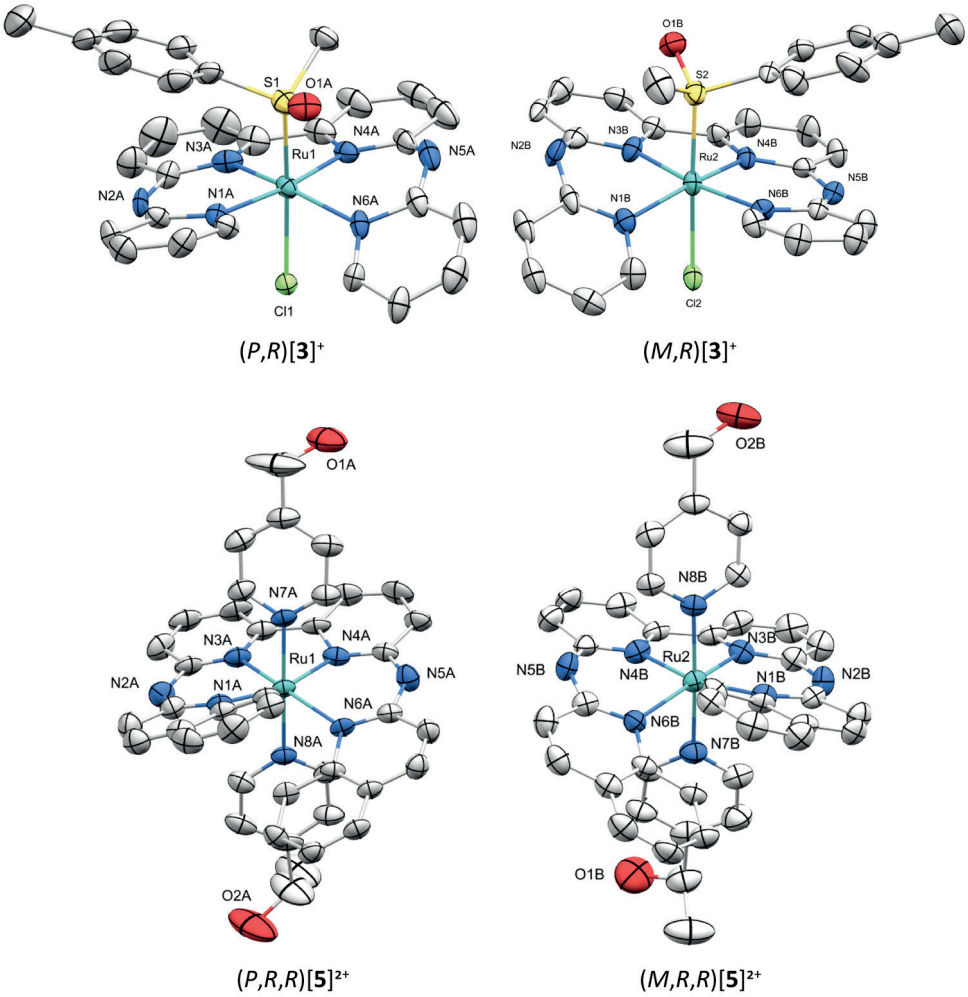

Figure SII.1. Displacement ellipsoid plots (50% probability level) for (*P*,*R*) and (M,R) diastereomers of [**3**]PF_6 and (*P*,*R*,*R*) and (*M*,*R*,*R*) epimers of [**5**]$(PF_6)_2$ at 110(2) K. Counter ions and hydrogens have been omitted for clarity.

HPLC

Sample Name:	**CG-85**	*Inj. Vol.:*	**25.0**
Sample Type:	**unknown**	*Dilution Factor:*	**1.0000**
Program:	**CJ-Chiral-prep-seperation-2mlmin**	*Operator:*	**n.a.**
Inj. Date/Time:	**16.11.21 15:06**	*Run Time:*	**20.09**

No.	Time min	Peak Name	Type	Area mAU*min	Height mAU	Amount n.a.
		TOTAL:		0.00	0.00	0.00

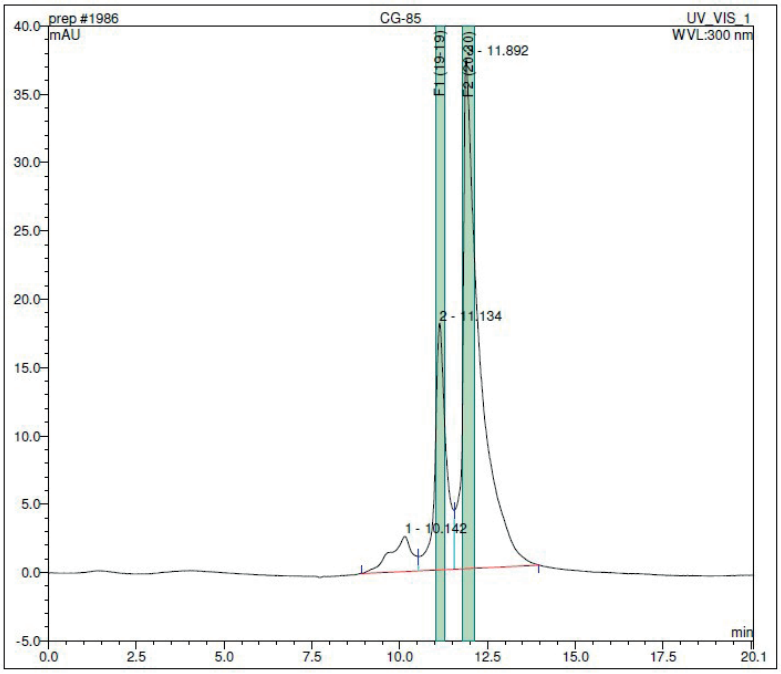

Figure SII.2. HPLC traces of [**4**]Cl with 0.1 M NH4Cl in MeOH eluent on the cyclobond I 2000 DMP column.

Appendix III: supporting information for chapter 4

Crystal structure

Table SIII.1. Selected distances and angles found for crystal structures of [**6**]$^{2+}$

Compound	[**6**]$^{2+,a}$
Ru1-N1	2.060(5)
Ru1-N2	1.968(5)
Ru1-N3	2.089(5)
Ru1-N4	2.118(5)
Ru1-N7	2.103(5)
Ru1-N8	2.065(5)
N1- Ru1-N3	158.7(2)
N7- Ru1-N8	79.0(2)

[a] Consists of two crystallographically independent formular units for the structure. The bond distance and angles are given for molecule A.

Photochemical characterization

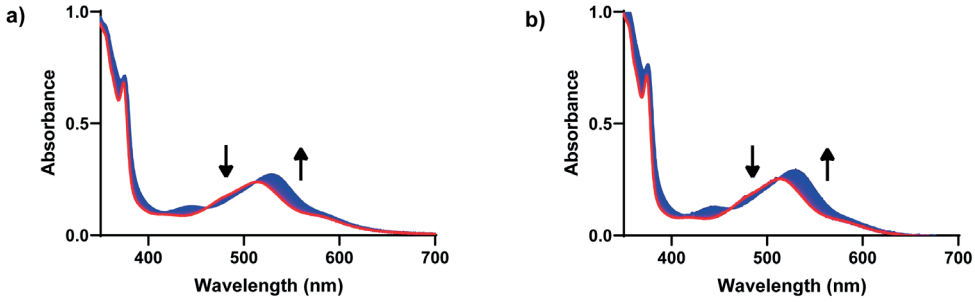

Figure SIII.1. a) Time evolution of the absorbance spectrum of compound [**2**]Cl_2 in MeCN (32 µM) upon green light (520 nm) irradiation, photon flux $5.7 \cdot 10^{-9}$ mol s^{-1}, T = 295 K. b) Time evolution of the absorbance spectrum of compound [**3**]Cl_2 in MeCN (34 µM) upon green light (520 nm) irradiation, photon flux $5.7 \cdot 10^{-9}$ mol s^{-1}, T = 295 K.

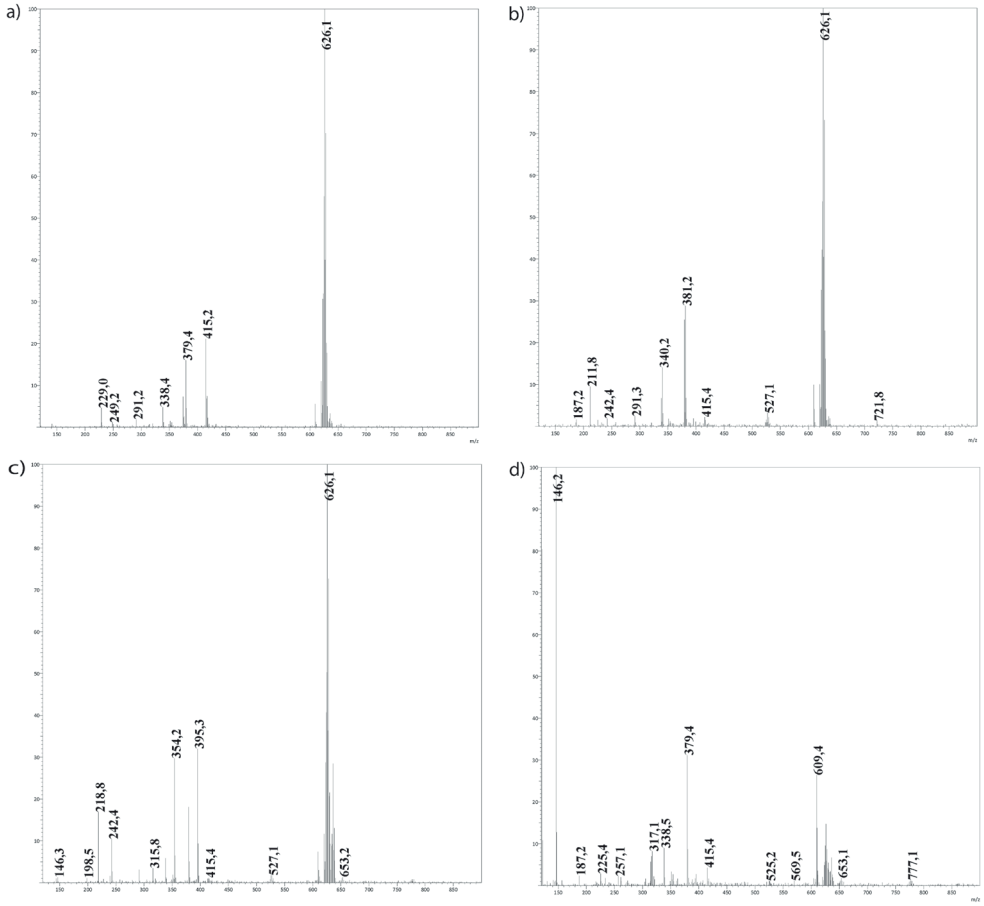

Figure SIII. 2. ES-MS spectra of the reaction mixture after photoreaction for [**1**]Cl_2 (a), [**2**]Cl_2 (b), [**3**]Cl_2 (c), [**4**]Cl_2 (d)

Facs

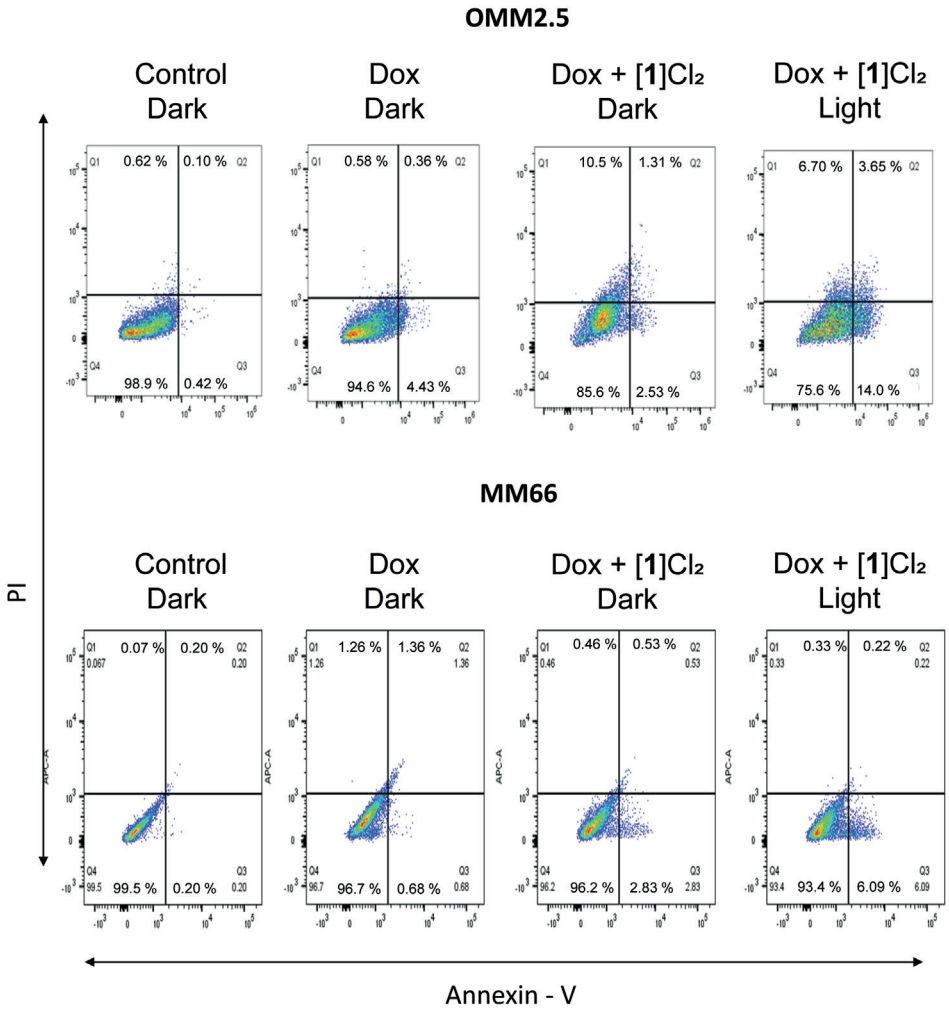

Figure SIII.3. Quantification of apoptosis by FACS in OMM2.5 and MM66 cells co-treated with [**1**]Cl_2 (50 µm) and Dox (500 nm) using Annexin V and Propidium Iodide (PI) staining. The cells were treated at t = 24 h with compound [**1**]Cl_2 followed by the addition of Dox (500 nM) at t = 48 h and light irradiation of 15 min green light (13.1 J/cm²). At t = 72 h the cells were prepared for FACS analysis.

Appendix IV: supporting information for chapter 5

NMR experiments

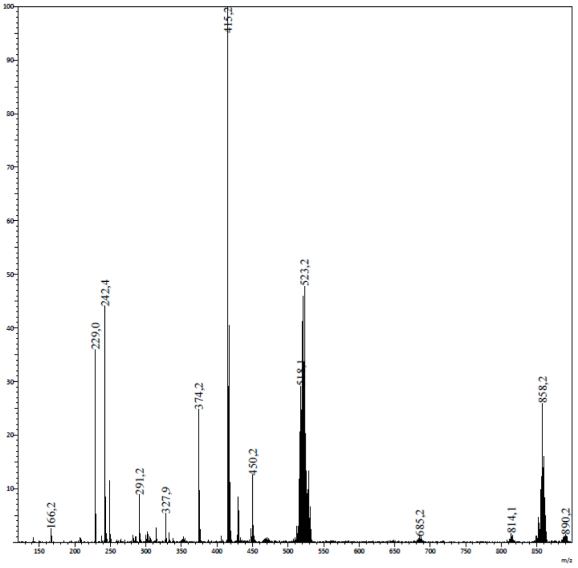

Figure SIV.1. ESI-MS measurement of the reaction product time evolution ^{1}H-NMR experiment of compound [**1**]Cl_2

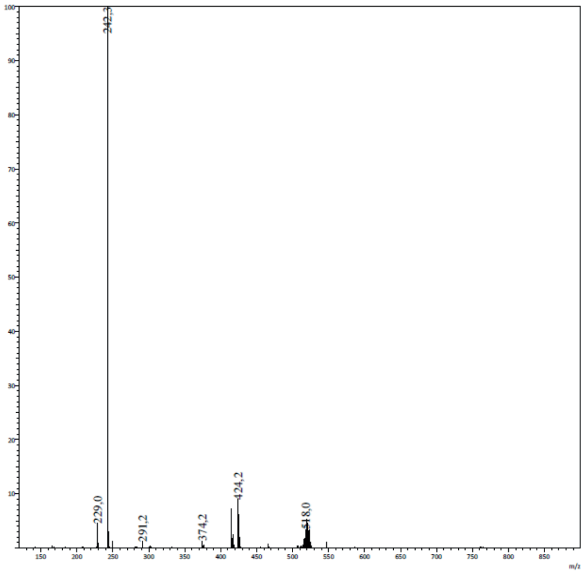

Figure SIV.2. ESI-MS measurement of the reaction product time evolution ^{1}H-NMR experiment of compound [**6**]Cl_2

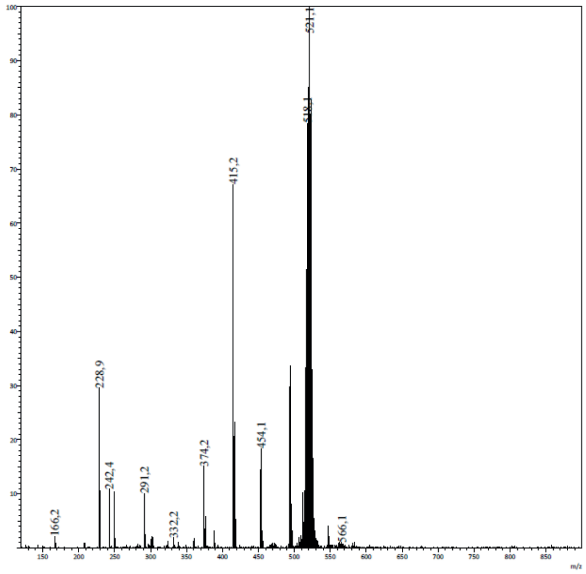

Figure SIV.3. ESI-MS measurement of the reaction product time evolution ^{1}H-NMR experiment of compound [**7**]Cl_2

Quantum yield experiments

$[Ru(bapbpy)(B02)_2]Cl_2$ [2]Cl_2

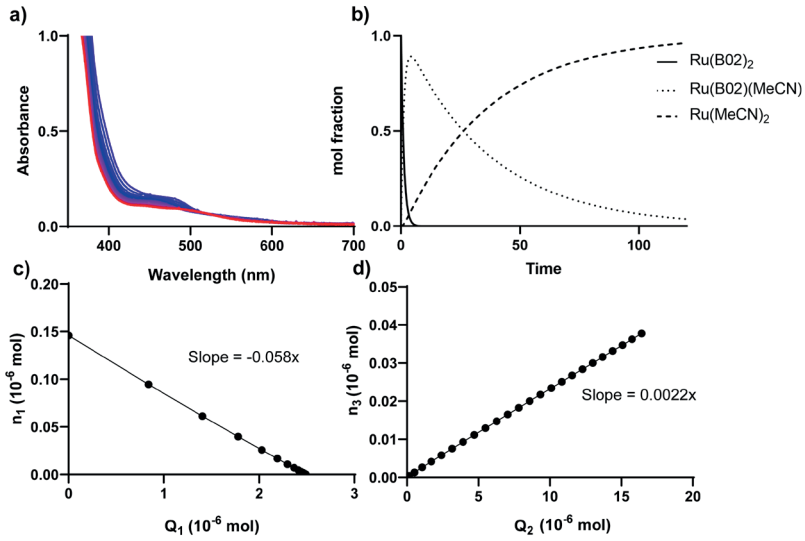

Figure SIV.4. a)Time evolution spectra of [**2**]Cl_2 upon blue light irradiation (435 nm), b) reaction profile calculated by gloteran for [**2**]Cl_2, c) Amount of $Ru(B02)_2$ (n_1) in mol vs absorbed photons by $Ru(B02)_2$ (Q_1) in mol, where the slope is the quantum yield of the first substitution reaction. d) Amount of $Ru(MeCN)_2$ (n_3) in mol vs absorbed photons by Ru(B02)(MeCN) (Q_2) in mol, where the slope is the quantum yield of the second substitution reaction.

[Ru(bapbpy)(B0Ref)$_2$]Cl$_2$ [3]Cl$_2$

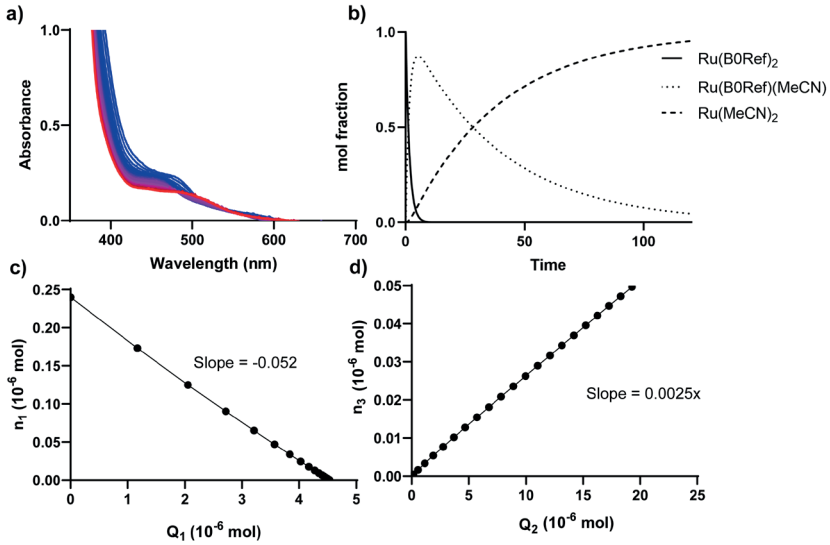

Figure SIV.5. a)Time evolution spectra of [**3**]Cl$_2$ upon blue light irradiation (435 nm), b) reaction profile calculated by gloteran for [**3**]Cl$_2$, c) Amount of Ru(B0Ref)$_2$ (n_1) in mol vs absorbed photons by Ru(B0Ref)$_2$ (Q_1) in mol, where the slope is the quantum yield of the first substitution reaction. d) Amount of Ru(MeCN)$_2$ (n_3) in mol vs absorbed photons by Ru(B0Ref)(MeCN) (Q_2) in mol, where the slope is the quantum yield of the second substitution reaction.

[Ru(bapbpy)(Py)$_2$]Cl$_2$ [4]Cl$_2$

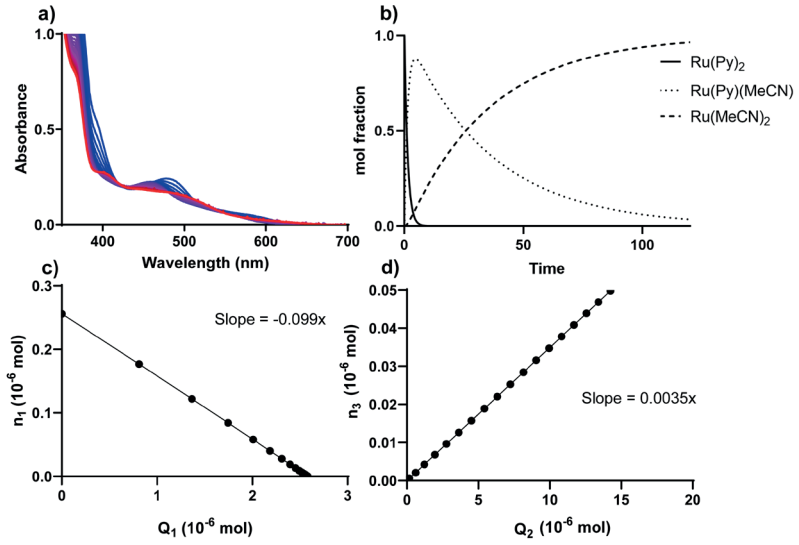

Figure SIV.6. a)Time evolution spectra of [**4**]Cl$_2$ upon blue light irradiation (435 nm), b) reaction profile calculated by gloteran for [**4**]Cl$_2$, c) Amount of Ru(Py)$_2$ (n_1) in mol vs absorbed photons by Ru(Py)$_2$ (Q_1) in mol, where the slope is the quantum yield of the first substitution reaction. d) Amount of Ru(MeCN)$_2$ (n_3) in mol vs absorbed photons by Ru(Py)(MeCN) (Q_2) in mol, where the slope is the quantum yield of the second substitution reaction.

[Ru(bapbpy)(B0Cl)(STF31)]Cl_2 [6]Cl_2

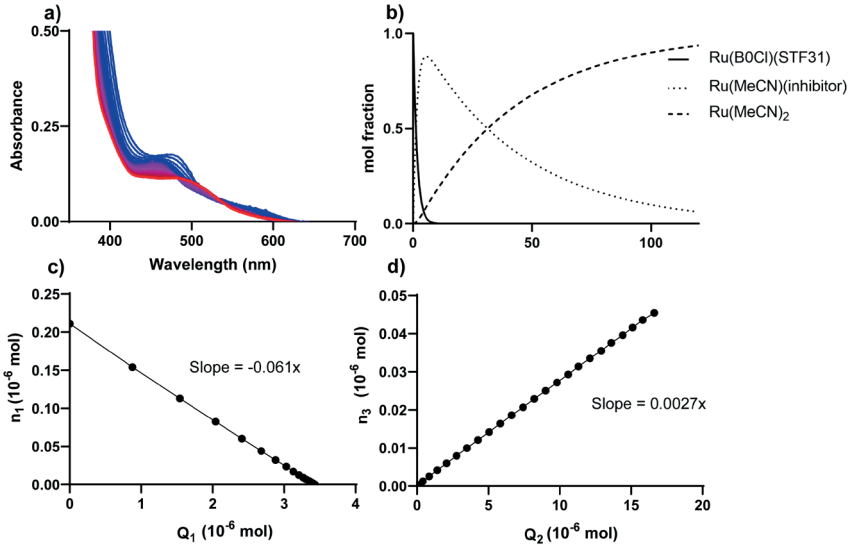

Figure SIV.7. a)Time evolution spectra of [**1**]Cl_2 upon blue light irradiation (435 nm), b) reaction profile calculated by gloteran for [**1**]Cl_2, c) Amount of Ru(B0Cl)(STF31) (n_1) in mol vs absorbed photons by (B0Cl)(STF31) (Q_1) in mol, where the slope is the quantum yield of the first substitution reaction. d) Amount of $Ru(MeCN)_2$ (n_3) in mol vs absorbed photons by (MeCN)(inhibitor) (Q_2) in mol, where the slope is the quantum yield of the second substitution reaction.

[Ru(bapbpy)(B0Cl)(PIK71)]Cl_2 [7]Cl_2

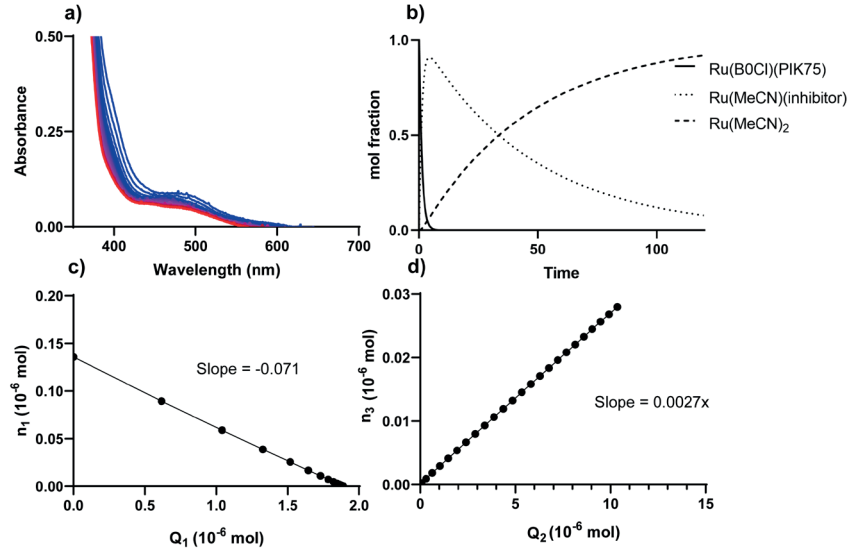

Figure 8. a)Time evolution spectra of [**7**]Cl_2 upon blue light irradiation (435 nm), b) reaction profile calculated by gloteran for [**7**]Cl_2, c) Amount of Ru(B0Cl)(PIK75) (n_1) in mol vs absorbed photons by (B0Cl)(PIK75) (Q_1) in mol, where the slope is the quantum yield of the first substitution reaction. d) Amount of $Ru(MeCN)_2$ (n_3) in mol vs absorbed photons by (MeCN)(inhibitor) (Q_2) in mol, where the slope is the quantum yield of the second substitution reaction.